AMERICAN SOCIETY FOR MICROBIOLOGY | Infection and Immunity

The Helical Shape of *Campylobacter jejuni* Promotes *In Vivo* Pathogenesis by Aiding Transit through Intestinal Mucus and Colonization of Crypts

Martin Stahl,[a] Emilisa Frirdich,[b] Jenny Vermeulen,[b] Yuliya Badayeva,[a] Xiaoxia Li,[c] Bruce A. Vallance,[a] Erin C. Gaynor[b]

Division of Gastroenterology, BC's Children's Hospital, the Child and Family Research Institute and the University of British Columbia, Vancouver, British Columbia, Canada[a]; Department of Microbiology and Immunology, University of British Columbia, Vancouver, British Columbia, Canada[b]; Department of Immunology, Cleveland Clinic Foundation, Cleveland, Ohio, USA[c]

***Campylobacter jejuni* is a helix-shaped enteric bacterial pathogen and a common cause of gastroenteritis. We recently developed a mouse model for this human pathogen utilizing the SIGIRR-deficient mouse strain, which exhibits significant intestinal inflammation in response to intestinal *C. jejuni* infection. In the current study, this mouse model was used to define whether *C. jejuni*'s characteristic helical shape plays a role in its ability to colonize and elicit inflammation in the mouse intestine. Mice were infected with the previously characterized straight-rod Δ*pgp1* and Δ*pgp2* mutant strains, along with a newly characterized curved-rod Δ*1228* mutant strain. We also compared the resultant infections and pathology to those elicited by the helix-shaped wild-type *C. jejuni* and complemented strains. Despite displaying wild-type colonization of the intestinal lumen, the straight-rod Δ*pgp1* and Δ*pgp2* mutants were essentially nonpathogenic, while all strains with a curved or helical shape retained their expected virulence. Furthermore, analysis of *C. jejuni* localization within the ceca of infected mice determined that the primary difference between the rod-shaped, nonpathogenic mutants and the helix-shaped, pathogenic strains was the ability to colonize intestinal crypts. Rod-shaped mutants appeared unable to colonize intestinal crypts due to an inability to pass through the intestinal mucus layer to directly contact the epithelium. Together, these results support a critical role for *C. jejuni*'s helical morphology in enabling it to traverse and colonize the mucus-filled intestinal crypts of their host, a necessary step required to trigger intestinal inflammation in response to *C. jejuni*.**

Campylobacter jejuni is a Gram-negative, microaerophilic bacterium and a common cause of infectious gastroenteritis. It possesses bipolar flagella and is highly motile. One of its defining characteristics is its helical shape, from which its name is derived. Although some rod-shaped *Campylobacter* species have been described (such as *C. hominis*, *C. showae*, *C. ureolyticus*, *C. concisus*, and *C. gracilis* [1, 2]), and rod-shaped variants of *C. jejuni* have been isolated (3), these appear to be the exception, with the helical shape being the standard morphology for *C. jejuni* as well as a number of related species among the epsilonproteobacteria, such as the gastric pathogen *Helicobacter pylori*.

The shape of a bacterial cell is maintained by its peptidoglycan (PG) layer (4). While many bacteria have a relatively simple coccoid or bacillus shape, modification of the PG layer can allow for the creation of more complex cell shapes such as the helix (5, 6). PG-modifying enzymes have been described as being responsible for generating the helical shape of *H. pylori* (Csd1, Csd2, Csd3/HdpA, Csd4, and Csd6) (7–13) and *C. jejuni* (Pgp1 and Pgp2) (14, 15). Pgp1 and Pgp2 are homologs of *H. pylori* Csd4 and Csd6, respectively. In addition, homologs of the *H. pylori* Csd1 and Csd3/HdpA proteins have also been identified in *C. jejuni*, and characterization is ongoing (E. Frirdich and E. C. Gaynor, unpublished data). Each of these enzymes is responsible for cleaving peptidoglycan peptide side chains. Pgp1 is a DL-carboxypeptidase that cleaves monomeric tripeptides into dipeptides, whereas Pgp2 is an LD-carboxypeptidase that cleaves both monomeric and cross-linked tetrapeptides into tripeptides. Deletion of the *pgp1* and *pgp2* genes results in the loss of cell curvature, forming *C. jejuni* cells with a rod-shaped morphology instead of the typical helical shape (14, 15).

From a functional standpoint, the role and evolutionary conservation of *C. jejuni*'s helical shape have been the subject of much speculation, but little direct experimentation. The *C. jejuni* helical morphology and polar flagella are thought to be responsible for the darting motility that this organism exhibits in high-viscosity media (16). Motility is a critical factor for *C. jejuni* colonization and pathogenesis, with nonmotile strains being severely impaired in their ability to colonize the intestines of their hosts (17–19). *C. jejuni* flagella are important not only for motility but also for adhesion and invasion into epithelial cells (20, 21) and for the delivery of effector molecules into host cells by serving as a type 3 secretion system (22). The helical shape of *C. jejuni* also plays a role in motility. The rod-shaped Δ*pgp1* and Δ*pgp2* mutants, having lost their helical shape, show slightly attenuated motility in soft agar (14, 15).

Received 30 August 2016 **Accepted** 10 September 2016

Accepted manuscript posted online 19 September 2016

Citation Stahl M, Frirdich E, Vermeulen J, Badayeva Y, Li X, Vallance BA, Gaynor EC. 2016. The helical shape of *Campylobacter jejuni* promotes *in vivo* pathogenesis by aiding transit through intestinal mucus and colonization of crypts. Infect Immun 84:3399–3407. doi:10.1128/IAI.00751-16.

Editor: S. R. Blanke, University of Illinois Urbana

Address correspondence to Bruce A. Vallance, bvallance@cw.bc.ca, or Erin C. Gaynor, egaynor@mail.ubc.ca.

M.S. and E.F. contributed equally.

Supplemental material for this article may be found at http://dx.doi.org/10.1128/IAI.00751-16.

One well-studied example of helix-shaped bacteria is the *Spirochaetes*, such as *Leptospira* spp. or *Borrelia* spp., which have internal periplasmic flagella between the cell wall and outer membrane that give the bacterial cell a long helical shape (23, 24). The rotation of the helix-shaped cell allows it to move rapidly, without the need for an external, rotating flagellum like that of other bacteria. Several studies have identified this system as a particularly efficient means of moving through a viscous medium by allowing the rotating helix-shaped cell to interact with large molecules within the medium as a means to generate the torque necessary to propel itself forward (25). Although both *C. jejuni* and the closely related *H. pylori* are nonmotile without their external flagella, the rotating motion of their helix-shaped cells may also boost their movement through viscous media, such as mucus. Intestinal mucus is a large network of interlocking glycoproteins, which create a thick, viscous, almost gel-like layer lining the intestinal epithelium and filling the lumen of intestinal crypts. Presumably, for *C. jejuni* to reach the intestinal epithelium and cause disease, it must find a way to overcome and cross this dynamic barrier. Indeed, studies on the movement of *C. jejuni* through viscous media found that *C. jejuni* exhibits a higher velocity in viscous media than in conventional liquid media, showing that it is well adapted to this type of environment (26, 27).

While previous studies examining the effects of cell shape on *Campylobacter* pathogenicity have been limited, studies with the Δ*pgp1* and Δ*pgp2* rod-shaped deletion mutants have indicated defects in chick colonization, altered activation of the human nucleotide-binding oligomerization domain-containing protein 1 (Nod1) by Δ*pgp1* and Δ*pgp2* strain PG, and a reduction in the release of the proinflammatory chemokine interleukin-8 (IL-8) from epithelial cells infected with the Δ*pgp1* mutant (14, 15). Neither Δ*pgp1* nor Δ*pgp2* mutants showed a defect in their ability to survive within intestinal epithelial cells (14, 15). Comparable studies on the role of *Helicobacter*'s helical shape have also yielded insights into the effect of PG modification and cell shape on the pathogenesis of this organism. Sycuro et al. identified 5 *H. pylori* genes (*csd1* to *-5*) (7, 8) that, when deleted, resulted in a loss of various degrees of helical cell shape. Each of these enzymes was shown to act by cleaving PG peptide side chains at specific points, thereby shifting the curvature of the cell. Each of the *csd1* to *-5* deletion mutants, when tested *in vivo*, displayed a significant competitive disadvantage in comparison to the wild type in colonization of the mucus layer of the mouse stomach (7, 8).

Mice deficient (−/−) in the single-IgG IL-1-related receptor (SIGIRR), a negative regulator of MyD88-dependent signaling (28), exhibit increased signaling by MyD88-dependent innate immune receptors and, interestingly, also display enhanced susceptibility to colonization/infection by a number of enteric pathogens, including *C. jejuni* (18). Relative to wild-type C57BL/6 mice infected with *C. jejuni*, *Sigirr*$^{-/-}$ mice (on a C57BL/6 genetic background) exhibit significantly increased inflammation at the principal sites of *C. jejuni* colonization in the cecum and proximal colon, despite similar pathogen burdens recovered from the two mouse strains. The intestinal inflammation that develops in the *C. jejuni*-infected *Sigirr*$^{-/-}$ mice appears to depend on activation of the innate receptor TLR4, since mice deficient in both SIGIRR and TLR4 were largely asymptomatic after *C. jejuni* infection. Conversely, mice lacking both SIGIRR and the innate receptor TLR2 displayed more severe intestinal inflammation than both wild-type mice and *Sigirr*$^{-/-}$ mice, possibly due to the increased barrier permeability in the gut associated with TLR2 deficiency (18).

In this study, we investigated the effects of the loss or alteration of *C. jejuni*'s helical cell shape in the *Sigirr*$^{-/-}$ mouse model of *C. jejuni* colonization and infection using rod-shaped Δ*pgp1* and Δ*pgp2* mutants and a previously uncharacterized curved-rod mutant lacking the *cjj81176_1228* gene (here referred to as the *1228* gene). The rod-shaped Δ*pgp1* and Δ*pgp2* mutants were largely nonpathogenic and unable to induce an inflammatory response, even in the highly susceptible *Sigirr*$^{-/-}$ mouse model. Conversely, the curved-rod Δ*1228* mutant and the complemented Δ*pgp1* and Δ*pgp2* strains with a restored helical shape displayed wild-type levels of inflammation in the *Sigirr*$^{-/-}$ mouse model. Furthermore, the nonpathogenic phenotype of the Δ*pgp1* and Δ*pgp2* mutants was attributed to the inability of rod-shaped *C. jejuni* strains to colonize the intestinal crypts. This supports the proposed link between *C. jejuni* helical cell shape and its pathogenic potential.

MATERIALS AND METHODS

Bacterial strains and growth conditions. The bacterial strains and plasmids used in this study, as well as their construction, are described in the supplemental methods and Table S1A in the supplemental material. Primers are listed in Table S2. Unless otherwise stated, *C. jejuni* strains were grown at 38°C in Mueller-Hinton (MH; Oxoid) broth or 8.5% (wt/vol) agar supplemented with vancomycin (10 μg/ml) and trimethoprim (5 μg/ml) under microaerobic/capnophilic conditions (6% O_2, 12% CO_2) in a Sanyo tri-gas incubator for plates or using the Oxoid CampyGen system for broth cultures. Growth media were supplemented with chloramphenicol (Cm; 20 μg/ml) or kanamycin (Km; 50 μg/ml) where appropriate. *Escherichia coli* strains used for plasmid construction were grown at 38°C in Luria-Bertani (LB; Sigma) broth or 7.5% (wt/vol) agar and supplemented with ampicillin (Ap; 100 μg/ml), Cm (15 μg/ml), or Km (25 μg/ml) as necessary.

***In vitro* invasion and intracellular survival in epithelial cell lines and IL-8 secretion.** The human INT407 epithelial cell line was used for *in vitro C. jejuni* infection experiments and grown as directed by the ATCC. In brief, cells were seeded into 24-well tissue culture plates at semiconfluence at ~1.5×10^5 cells/ml. Infections were carried out as previously described (14). Adherence and invasion were measured at 3 h postinfection, invasion was measured at 5 h postinfection, and intracellular survival was measured at 8 h and 24 h postinfection. The concentration of IL-8 secreted by INT407 human epithelial cells either left uninfected or infected with *C. jejuni* wild-type strain 81-176 or the Δ*pgp1*, Δ*pgp2* Δ*1228*, or Δ*1228*c strain was assayed using the human IL-8 enzyme-linked immunosorbent assay (ELISA) kit (Invitrogen, Camarillo, CA) per the manufacturer's instructions (14).

Motility assays. Motility assays in soft agar were carried out with strains grown in shaking MH-TV broth for 18 h as described previously (14). These cultures were diluted in MH-TV broth to an optical density at 600 nm (OD_{600}) of 0.2, and 2 μl of this culture was point inoculated into MH-TV plates containing 0.4% agar. The plates were incubated for 20 h under microaerobic conditions, and the diameter of the growth halo extending from the inoculation point was measured. Motility in liquid medium was assessed based on previously established methods (27). In brief, *C. jejuni* strains were inoculated into 0.4% soft agar MH plates and then grown for 48 h at 37°C under microaerobic conditions. A sterile loop was used to sample *C. jejuni* from the outer edge of the growth ring, and the samples were then resuspended in 100 μl of prewarmed MH medium. Fifty microliters was pipetted onto a prewarmed microscope slide, and the bacteria were visualized using a Zeiss AxioImager Z1 microscope under ×630 magnification. Zeiss AxioVision software was used to image bacterial movement on the slide for 6 s with a time lapse of 0.2 s per frame. The same software was used to measure the distance traveled by individual bacterial cells between frames, and their velocity was calculated in mi-

crometers per second. Statistical significance between strains was determined using a nonparametric Kruskal-Wallis one-way test for variance ($P < 0.05$).

Mouse strains and infection experiments. The wild-type C57BL/6 and *Sigirr*$^{-/-}$ mouse strains used in this study were all bred in-house and kept under specific-pathogen-free conditions at the Child and Family Research Institute (CFRI). Mice at 6 to 10 weeks of age were orally gavaged with 100 μl of a 50-mg/ml vancomycin solution suspended in phosphate-buffered saline (PBS) (dose per mouse of ~5 mg), 4 h prior to inoculation with 100 μl of an overnight *C. jejuni* culture (~10^7 CFU per dose). The initial weight of each mouse was recorded, and weight was monitored regularly throughout the infection. Seven days postinfection, mice were anesthetized with isoflurane and euthanized by cervical dislocation. The mice were immediately dissected, and their cecum was isolated. Sections of cecal tissues were fixed in 10% neutral buffered formalin (Fisher) for later histological analysis. The remainder of the cecum (including luminal contents) and other isolated tissues were suspended in 1 ml sterile PBS (pH 7.4) for viable *C. jejuni* counts. Tissue samples were homogenized, serially diluted, and plated onto *Campylobacter* agar plates containing Karmali selective supplements (Oxoid). Following 48 h of incubation at 42°C under microaerobic conditions, *C. jejuni* colonies were enumerated, and the pathogen burdens (CFU per gram of tissue) were calculated. Statistically significant differences were determined using a nonparametric Mann-Whitney test, with a *P* value of <0.05 used as the threshold for significance.

Ethics statement. All animal experiments were performed according to protocol number A11-290, approved by the University of British Columbia's Animal Care Committee and in direct accordance with the Canadian Council of Animal Care (CCAC) guidelines. Mice were monitored daily for mortality and morbidity throughout their infection and euthanized if they showed signs of extreme distress or more than 15% body weight loss.

Histology, pathological scoring, and immunofluorescent staining. Murine cecal tissue samples were fixed in 10% formalin at the time of euthanization and were paraffin embedded and cut for further histological analysis. The paraffin-embedded tissue sections were stained with hematoxylin and eosin, photographed, and then used for pathological scoring. Pathology scoring was done by two blinded observers, according to previously established criteria (18). Briefly, each tissue section was assessed for (i) submucosal edema (0, no change; 1, mild; 2, moderate; 3, severe), (ii) crypt hyperplasia (0, no change; 1, 1 to 50%; 2, 51 to 100%; 3, >100%), (iii) goblet cell depletion (0, no change; 1, mild depletion; 2, severe depletion; 3, absence of goblet cells), (iv) epithelial integrity (0, no pathological changes detectable; 1, epithelial desquamation [few cells sloughed, surface rippled]; 2, erosion of epithelial surface [epithelial surface rippled, damaged]; 3, epithelial surface severely disrupted/damaged, large amounts of cell sloughing; 4, ulceration [with an additional score of 1 added for each 25% fraction of tissue in the cross section affected up to a maximum score of 8 {4 + 4} for a tissue section that had entirely lost its crypt structure due to epithelial cell loss and immune cell infiltration]), (v) mucosal mononuclear cell infiltration (per ×400 magnification field) (0, no change; 1, <20; 2, 20 to 50; 3, >50 cells/field), and (vi) submucosal polymorphonuclear leukocyte (PMN) and mononuclear cell infiltration (per ×400 magnification field) (1, <5; 2, 21 to 60; 3, 61 to 100; 4, >100 cells/field). Statistical significance ($P < 0.05$) was determined using a two-way analysis of variance (ANOVA), with a Bonferroni posttest.

Immunofluorescent staining of the formalin-fixed, paraffin-embedded sections was conducted using previously established protocols (18). The primary antibodies used were raised against mucin 2 (rabbit polyclonal; Santa Cruz Biotechnology) and *C. jejuni* (biotin-rabbit polyclonal; Abcam). Each was visualized using Alexa Fluor 488-conjugated donkey anti-rabbit IgG (Invitrogen) or Alexa Fluor 568-conjugated streptavidin (Molecular Probes). The tissues were mounted using ProLong Gold antifade reagent containing 4′,6-diamidino-2-phenylindole (DAPI) (Invitrogen). The stained slides were viewed using a Zeiss AxioImager Z1 microscope and photographed using an AxioCam HRm camera with AxioVision software.

RESULTS

The *C. jejuni 81-176_1228* gene influences cell curvature and has effects on intracellular survival in epithelial cells. *C. jejuni* PG hydrolases Pgp1 (14) and Pgp2 (15) are involved in helical shape determination in this organism. Deletion mutations in these two genes result in the complete loss of *C. jejuni*'s curved shape, with the Δ*pgp1* mutant exhibiting a common bacillus shape, while the Δ*pgp2* mutant has a slightly more oval shape with narrowed ends. Complementation of both mutants restores wild-type helical morphology (14, 15).

In addition to the rod-shaped mutants, we included a curved-rod mutant. Several genes identified by bioinformatics analysis as putatively involved in PG modification, peptidase activity, and/or cell shape were deleted, many of which showed curved-rod phenotypes (Frirdich and Gaynor, unpublished). Of these curved-rod mutants, only a mutation in the *cjj81176_1228* gene (referred to here as *1228*) (Fig. 1A) resulted in a population with uniform cell morphology, whereas other mutants exhibited more pleomorphic cell shapes; thus, the Δ*1228* mutant was selected for further analysis in this study. The Δ*1228* mutant population morphology consisted of C-shaped and S-shaped cells with decreased helicity in comparison to wild-type *C. jejuni* and the previously published rod-shaped Δ*pgp1* and Δ*pgp2* mutants (Fig. 1B) (14, 15). The complemented strain, designated the Δ*1228*c strain, was created by expressing the *1228* gene at the rRNA spacer locus of the Δ*1228* strain. Wild-type cell morphology was restored in the Δ*1228*c strain (Fig. 1B). The *1228* gene product is annotated as a putative peptidase with a C-terminal domain belonging to the M23 peptidase family of zinc metallopeptidases that includes PG endopeptidases, as determined by conserved domain analysis. It also shows 46% identity/65% similarity with *H. pylori* G27 Csd3/HdpA (7) and 45% identity/64% similarity with *H. pylori* 26695 Csd3/HdpA (9), each of which has been described as being important in controlling the helical cell shape in *H. pylori*. Conserved domain analysis and sequence similarity to *H. pylori* Csd3/HdpA, as well as the shape of the deletion mutant, indicate that 1228 is likely a PG peptidase; however, its exact function has yet to be determined, so at present the *1228* gene has not been given a *pgp* (peptidoglycan peptidase) designation like *pgp1* and *pgp2*.

As published previously, neither the Δ*pgp1* nor Δ*pgp2* mutant displayed any impairment in cell adhesion, invasion, or intracellular survival (14, 15); (see Fig. S1A in the supplemental material), which are commonly used indicators for *C. jejuni* pathogenicity. As a further indicator of *in vitro* pathogenesis, the infection of epithelial cells by *C. jejuni* is associated with the increased production and release of the chemokine IL-8 (29). The Δ*pgp1* mutant showed enhanced secretion from INT407 cells of the IL-8 chemokine in comparison to wild type, while the Δ*pgp2* mutant showed a response identical to that of the wild type, as previously published (14) (see Fig. S1B). To evaluate how these results compared to the Δ*1228* mutant, we tested the ability of the Δ*1228* mutant to adhere to, invade, and survive within human intestinal epithelial cells and determined the levels of IL-8 secreted by epithelial cells infected with the Δ*1228* mutant. Epithelial cell infections were carried out using the INT407 cell line in a gentamicin protection assay, as was done previously for the Δ*pgp1* or Δ*pgp2* strain. Unlike the Δ*pgp1* and Δ*pgp2* mutants (14, 15) (see Fig. S1A), the

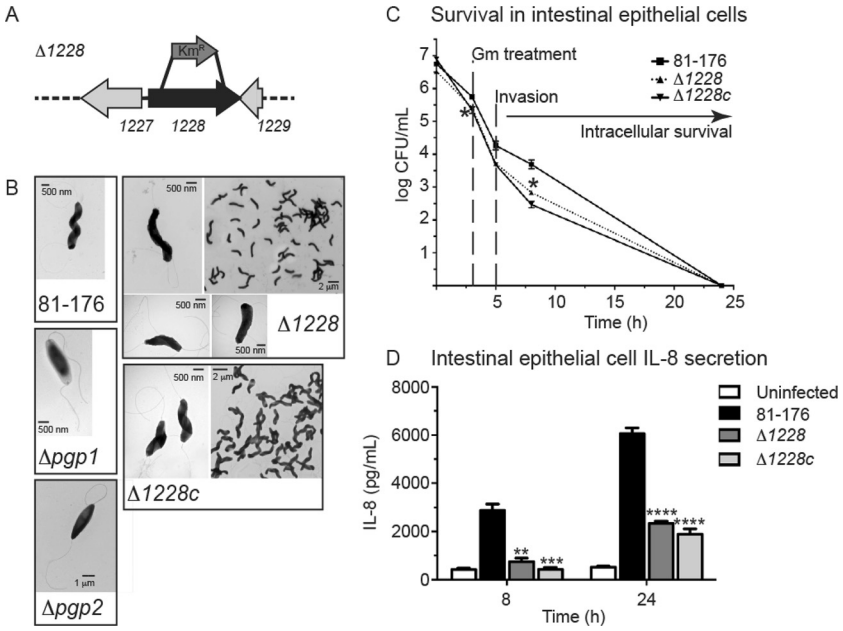

FIG 1 *C. jejuni cjj81176_1228* (*1228*) gene locus and morphology, invasion and intracellular survival, and IL-8 secretion levels of the Δ*1228* strain. (A) Genomic organization of *cjj81176_1228* (denoted as *1228*) gene locus. The Δ*1228* mutant strain was constructed by deleting 1,014 bp of the 1,161-bp gene and replacing it with the nonpolar *aphA3* Km^r cassette. (B) Negatively stained transmission electron microscopy images of the helical *C. jejuni* 81-176 strain, the rod-shaped Δ*pgp1* (14) and Δ*pgp2* (15) mutant strains, C- and S-shaped Δ*1228* mutant strain, and Δ*1228* complemented strain (Δ*1228*c) with restored helical morphology. All strains show intact flagella. (C) Invasion by and intracellular survival of the *C. jejuni* wild type 81-176 Δ*1228* mutant and Δ*1228* complemented strain (Δ*1228*c) in the INT407 epithelial cell line were assessed by the gentamicin (Gm) protection assay. The Δ*1228* mutant strain showed a slight defect in invasion and intracellular survival. Gm was added 3 h postinfection. After 2 h, the Gm was washed off and the cells were incubated with fresh MEM containing 3% fetal bovine serum and a low dose of Gm. At each time point, CFU were determined for each well by lysing the cells with water and plating the dilutions onto MH-TV plates. Data represent the mean ± standard error of the mean from three replicates and are representative of three independent experiments. (D) ELISA was used to quantify IL-8 levels secreted by uninfected INT407 epithelial cell lines and cells infected for 8 and 24 h with *C. jejuni* wild-type 81-176, Δ*1228*, and Δ*1228*c strains. The Δ*1228* mutant resulted in decreased IL-8 secretion in comparison to wild type. Data represent the mean ± standard error of the mean from three replicates and are representative of three independent experiments. Asterisks indicate a statistically significant difference using the unpaired Student *t* test, with *, **, ***, and **** indicating $P < 0.05$, $P < 0.01$, $P < 0.001$, and $P < 0.0001$, respectively.

Δ*1228* mutant exhibited a small defect in adherence, invasion, and intracellular survival (Fig. 1C), with an 0.4-log decrease in adherence and invasion at 3 h, an 0.5-log decrease in invasion at 5 h (not statistically significant), and an 0.9-log decrease in intracellular survival at 8 h in comparison to the wild type. No intracellular bacteria were recovered at 24 h. The invasion and intracellular survival defects could not be restored in a complemented strain, as has sometimes been observed previously (M. Pryjma and E. C. Gaynor, unpublished data). To determine whether the IL-8 secretion levels were altered during infection with a Δ*1228* mutant, INT407 human epithelial cells were infected with *C. jejuni* wild-type, Δ*1228*, and Δ*1228*c strains. The IL-8 levels released into the supernatant were then measured at 8 h and 24 h postinfection by ELISA (Fig. 1C). The Δ*1228* mutant strain showed a statistically significant 3.8- and 2.6-fold decrease in IL-8 secretion in comparison to wild-type *C. jejuni* at 8 h and 24 h, respectively. The complemented strain did not restore IL-8 secretion levels to wild-type levels. To determine why complementation failed to restore the wild-type phenotype in the Δ*1228* mutant, we assessed both the cell morphology and *1228* gene transcription of the complemented strain when grown in minimum essential medium (MEM; the growth medium for the cell invasion and IL-8 secretion assay) and MH broth (the medium used in all other assays that showed complementation). Wild-type cell morphology was restored when the complemented strain was grown in MH broth but not when the complement was incubated in MEM (see Fig. S2A). This does not appear to be due to various levels of the *1228* gene, as *1228* gene transcription remained constant in the Δ*1228*c strain in both MH broth and MEM (see Fig. S2B).

Shape mutants display motility defects in soft agar and viscous media but not in liquid media. A key *C. jejuni* pathogenicity determinant is its motility (30). Both Δ*pgp1* and Δ*pgp2* strains were identified as having defects in motility through soft agar (14, 15), so we tested whether the change in morphology of the Δ*1228* mutant also affected its motility in soft agar by measuring the diameter of the halo of growth following 24 h of incubation at 37°C. The soft agar motility of the Δ*1228* strain was on average 85.1% of that of the wild type (Fig. 2A), while those of Δ*pgp1* and Δ*pgp2* mutants were 81.0% and 66.3%, respectively (Fig. 2A), slightly lower than the previously published values of 82.5% and 73.7%, respectively (14, 15). The motility defect of the Δ*1228* strain was restored in the complemented strain (Fig. 2A).

The soft agar assay analyzes changes in *C. jejuni* motility through a semisolid gel. To remove the resistance of the agar and analyze motility in a nonviscous solution, we measured bacterial velocity in liquid MH medium using a standard light microscope by recording images at 0.2-s intervals under ×630 magnification. The movement of individual *C. jejuni* cells was plotted between frames, and their velocity was calculated in micrometers per second, similarly to previously published studies (27). Although

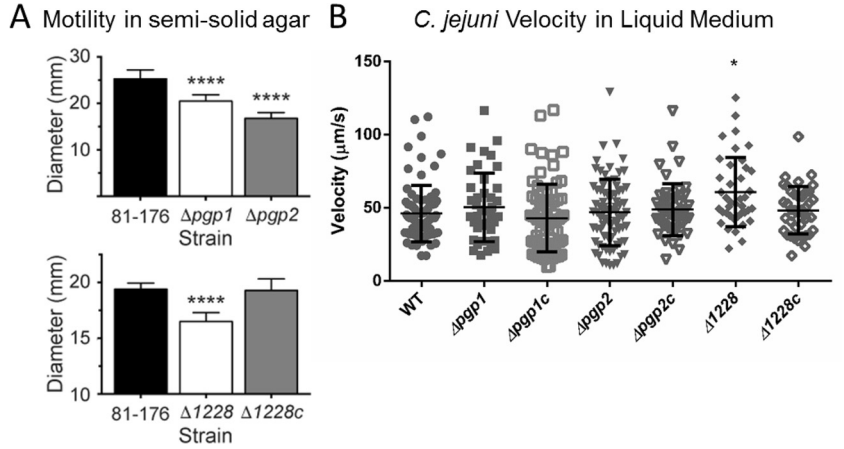

FIG 2 Motility of *C. jejuni* wild-type 81-176, Δ*pgp1*, Δ*pgp2*, Δ*1228*, and complemented strains. (A) As assayed by measuring halo diameters in soft agar plates, the Δ*pgp1*, Δ*pgp2*, and Δ*1228* mutants exhibited 81.0%, 66.3%, and 85.1% of wild-type motility, respectively. Complementation of the Δ*1228* mutant (Δ*1228*c) showed restoration of wild-type motility. Standard error of the mean was calculated from 9 measurements. The asterisks indicate a statistically significant difference using the unpaired Student *t* test, **** indicating a *P* value of <0.0001. (B) Motility of the wild-type, mutant, and complemented *C. jejuni* strains in liquid MH medium recorded over 6 s with a time-lapse of 0.2 s/frame. The velocity (micrometers per second) was calculated by measuring the distance moved by individual cells between frames, divided by the number of frames over which the movement was tracked. Statistical significance was determined using a Kruskal-Wallis test ($P < 0.05$).

there was a large amount of variability between individual cells, there was on average little difference between the wild-type and Δ*pgp1* and Δ*pgp2* mutant and complemented strains, with the exception of the Δ*1228* strain, which demonstrated on average a slight (10- to 15-μm/s) increase in motility relative to the wild type (Fig. 2B) ($P < 0.05$). With a loss of motility in soft agar but not in liquid media, the motility defect of the shape mutants is likely not due to a defect in flagellar rotation but rather a result of the changes in cell shape.

Rod-shaped Δ*pgp1* and Δ*pgp2* mutants, but not the curved Δ*1228* mutant, exhibit defective pathogenesis in *Sigirr*$^{-/-}$ mice. With the helical morphology of *C. jejuni* being presumed to be an important factor for intestinal colonization as well as motility within the mucus layer *in vivo*, we tested the colonization and pathology of the *C. jejuni* Δ*pgp1*, Δ*pgp2*, and Δ*1228* mutants in *Sigirr*$^{-/-}$ mice. We recently described this mouse strain as a powerful model for studying the pathology of *C. jejuni* colonization and infection (18). The increased susceptibility of these mice is due to the absence of SIGIRR, an inhibitor of most MyD88-dependent signaling. The result is a mouse model with increased signaling via TLR and IL-1R (31). TLR2 and TLR4 have been previously identified as being particularly relevant for *C. jejuni* infection (18, 32). When these mice are orally infected with *C. jejuni*, *C. jejuni* quickly colonizes the crypts as well as the mucus layer of the cecum and proximal colon, triggering an acute, self-limiting inflammatory reaction within the intestinal mucosa (18).

We pretreated groups of *Sigirr*$^{-/-}$ mice with 5 mg vancomycin, followed 4 h later by an inoculation of approximately 10^7 CFU of the wild-type *C. jejuni* 81-176 strain; the Δ*pgp1*, Δ*pgp2*, and Δ*1228* mutant strains; and the Δ*pgp1*c, Δ*pgp2*c, and Δ*1228*c complemented *C. jejuni* strains. The vancomycin pretreatment was used to abet consistent colonization by *C. jejuni* by reducing the number of commensal bacteria, thereby opening niches within the cecum for *C. jejuni* to colonize. When the mice were euthanized and their intestinal tissues were collected 7 days postinfection, each of the strains colonized the mouse cecum to approximately similar levels (10^9 CFU/g) (Fig. 3). The Δ*pgp1* and Δ*pgp2* mutants demonstrated a slight defect in mean colonization levels; however, this difference was not statistically significant (Fig. 3).

Despite similar colonization numbers, a marked difference was observed in the pathology elicited by the different strains (Fig. 4). In accordance with our previous studies (18), infection of *Sigirr*$^{-/-}$ mice by wild-type *C. jejuni* triggered significant inflammation and pathology in the cecum and proximal colons of infected mice. This was characterized by crypt epithelial hyperplasia, infiltration of the mucosa and submucosa by inflammatory and immune cells, and, in the worst cases, the development of mucosal ulcers (Fig. 4). In contrast, *Sigirr*$^{-/-}$ mice colonized by the Δ*pgp1* and Δ*pgp2* mutants showed very little, if any, inflam-

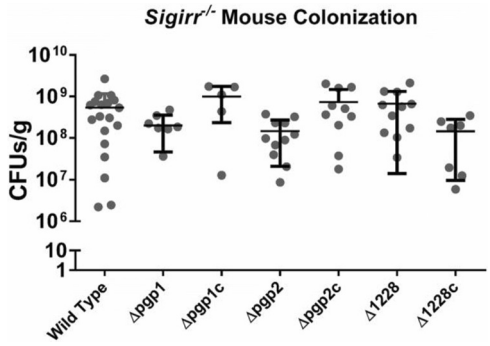

FIG 3 Colonization of *Sigirr*$^{-/-}$ mice by wild-type *C. jejuni* and mutant and complemented strains as CFU per gram recovered from the cecum of *Sigirr*$^{-/-}$ mice colonized by wild-type *C. jejuni* 81-176 and Δ*pgp1*, Δ*pgp2*, and Δ*1228* mutant strains and the Δ*pgp1*c, Δ*pgp2*c, and Δ*1228*c complemented strains, all at 7 days postinfection. Most colonization levels ranged between 10^8 and 10^9 CFU/g, with Δ*pgp1* and Δ*pgp2* mutants having on average a slightly reduced pathogen burden per gram of tissue/luminal contents compared with the other strains, although this was not statistically significant. Statistical significance was determined using a Mann-Whitney test ($P < 0.05$). No strains met this threshold.

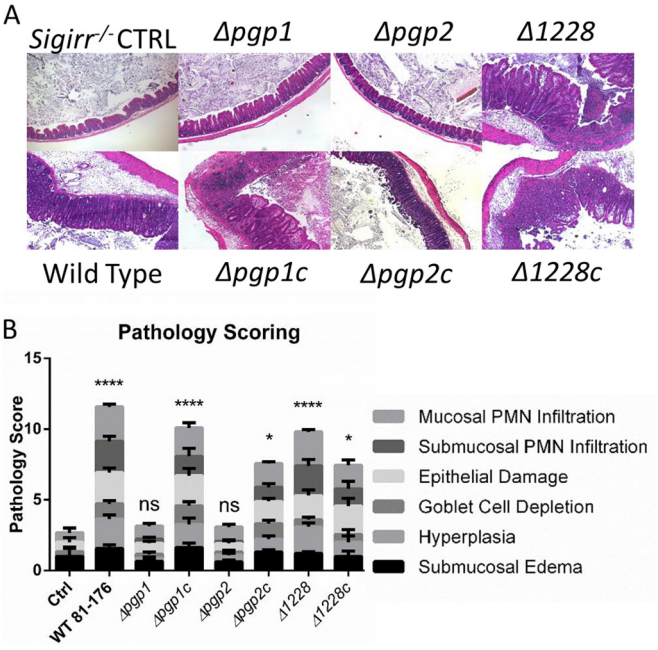

FIG 4 Tissue pathology in *C. jejuni*-infected *Sigirr*$^{-/-}$ mice. (A) Hematoxylin-and-eosin-stained histological sections from infected mouse ceca. Tissue samples were collected 7 days postinfection, formalin fixed, and paraffin embedded. Images were taken under ×100 magnification and were representative of tissues from at least seven mice. The uninfected control and Δ*pgp1* and Δ*pgp2* mutant-infected mice showed few signs of inflammation, whereas the ceca of mice infected with wild-type, Δ*1228*, and Δ*pgp1*c, Δ*pgp2*c, and Δ*1228*c complemented strains showed significant edema, crypt hyperplasia, and immune cell infiltration. (B) Pathological scoring was done by two blinded observers using hematoxylin-and-eosin-stained, formalin-fixed, cecal tissue sections. Scoring was done on a scale from 0 to 24, as described elsewhere (18). Significant pathology relative to uninfected controls was observed in mice infected with the wild type, the Δ*1228* strain, and all complemented strains. No significant pathology was observed in mice infected with the Δ*pgp1* and Δ*pgp2* mutant strains. Statistical significance was determined using a two-way analysis of variance and a Bonferroni posttest. ns, not statistically significant; *, $P > 0.05$; ****, $P > 0.0001$.

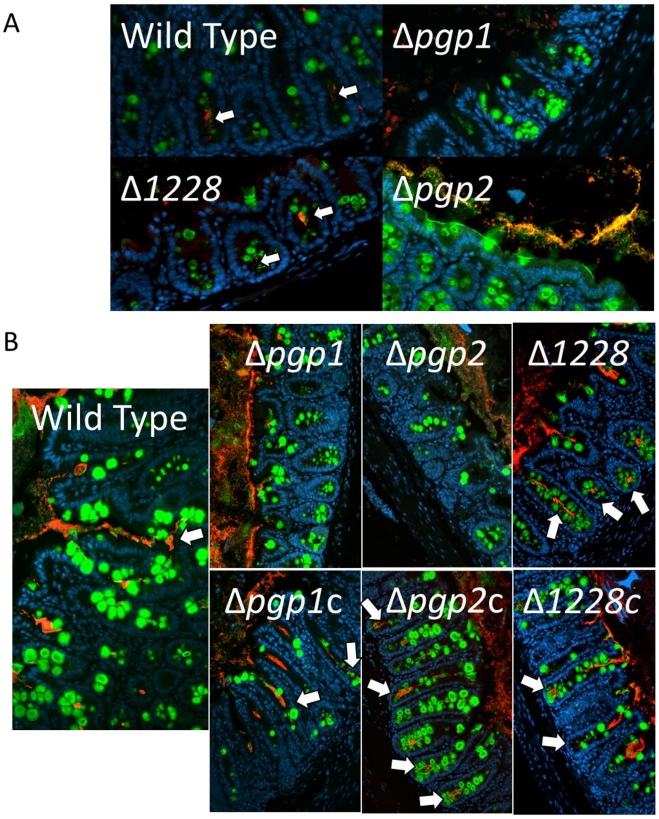

FIG 5 Immunofluorescent staining of *C. jejuni* cecal colonization in infected *Sigirr*$^{-/-}$ mice. Formalin-fixed, paraffin-embedded tissue sections of ceca obtained from *Sigirr*$^{-/-}$ mice infected with wild-type, mutant, or complemented strains of *C. jejuni* at 3 days postinfection (A) or 7 days postinfection (B), at ×200 magnification. Cell nuclei are stained with DAPI (blue), the goblet cells and secreted mucus are stained with antibodies specific to Muc2 (green), and *C. jejuni* is stained with *C. jejuni*-specific antibodies (red). The wild type, the Δ*1228* mutant, and all complemented strains are visible in the lumen, mucus layer, and crypts (white arrows). The Δ*pgp1* and Δ*pgp2* mutants are absent from the crypts.

mation following infection, as indicated by pathology scores similar to those of uninfected mice (CTRL in Fig. 4). In the complemented strains, the pathology in infected mice was restored to wild-type levels (Fig. 4). In contrast to the Δ*pgp1* and Δ*pgp2* mutants, *Sigirr*$^{-/-}$ mice infected with the curved Δ*1228* strain showed wild-type colonization levels and pathology, with pathology scores comparable to that of the wild-type strain (Fig. 3 and 4). Therefore, the Δ*1228* mutant does not appear to display any significant defects in eliciting gastrointestinal disease *in vivo* in *Sigirr*$^{-/-}$ mice (Fig. 4).

Rod-shaped mutants are impaired in intestinal crypt colonization. With substantially different pathologies elicited by the Δ*pgp1*, Δ*pgp2*, and Δ*1228* mutant strains 7 days postinfection, despite the mice carrying similar pathogen burdens, we further examined the reason for this difference. Previous work with both *Sigirr*$^{-/-}$ and conventional wild-type mice indicated that *C. jejuni* preferentially colonizes the mucus layer that overlies the intestinal epithelium, as well as filling intestinal crypts along the cecum and proximal colon, with large numbers of bacteria frequently seen accumulating within the mucus of the crypts (18, 33). The intestinal crypts are also presumably the site where the most direct interactions between *C. jejuni* and its host occur. Immunofluorescence was used to visualize the location of the colonizing bacteria relative to the intestinal epithelium of the host in formalin-fixed cecal and colonic tissue sections collected from infected *Sigirr*$^{-/-}$ mice 3 and 7 days postinfection (Fig. 5A and B). For all strains, *C. jejuni* pathogen burdens early in infection (up to 3 days postinfection) were relatively low and quite variable (data not shown) and signs of inflammation had not yet developed; however, even at these early stages of infection, we could detect *C. jejuni* in the lumen and/or crypts of the cecum and colon using immunofluorescence (Fig. 5A). At 3 and 7 days postinfection, the wild-type *C. jejuni* 81-176 strain infecting *Sigirr*$^{-/-}$ mice displayed similar deep penetration/colonization of intestinal crypts as previously reported (Fig. 5) (18, 33). In contrast, neither the Δ*pgp1* nor the Δ*pgp2* mutant colonized the intestinal crypts at any time point examined (Fig. 5). While these mutants were found lodged within the mucus layer lining the superficial epithelium facing the lumen (see Fig. S3), there was minimal penetration into intestinal crypts, with the base of the crypts being completely devoid of *C. jejuni* (Fig. 5). The Δ*pgp1* and Δ*pgp2* complemented strains showed crypt colonization levels comparable to that of the wild type. In

accordance with the pathology results obtained with the Δ*1228* mutant, the Δ*1228* mutant readily colonized the intestinal crypts at both 3 and 7 days postinfection and resembled the wild-type strain (Fig. 5). In the infected mice, the complemented Δ*1228*c strain was similar in both colonization and pathology to the Δ*1228* mutant and wild-type strains.

DISCUSSION

Like other enteric bacterial pathogens, before *C. jejuni* can establish an infection, it must first enter the gastrointestinal tract and then colonize an ecological niche from which it can proliferate and spread. The inability of nonmotile *C. jejuni* to efficiently colonize the host intestine indicates that motility is critical for colonization. Several lines of evidence suggest that in some mammalian hosts, such as mice, *C. jejuni* is ill suited to compete and survive among the resident commensals that colonize the intestinal lumen (18, 34, 35). Our mouse model of *C. jejuni* infection initially reduces this competitive pressure via the depletion of commensal microbes by preinoculation with vancomycin. Our model indicates that for intestinal pathology to develop during *C. jejuni* infection, *C. jejuni* needs to come into close proximity with the host epithelium, activating innate immune receptors such as TLR4 that help drive the host inflammatory response against *C. jejuni* (18, 32). Epithelial cell invasion, a common marker of *C. jejuni* pathogenesis, was also observed in infected *Sigirr*$^{-/-}$ mice (18, 33). In order to access the intestinal epithelial layer, *C. jejuni* has to enter and move within the overlying intestinal mucus. In addition to motility, *C. jejuni* chemotaxis toward mucus and its constituents (36), including mucin proteins and the common mucus-associated glycan L-fucose (37), is known to play an important role in *C. jejuni* colonization. We have also observed from our previous studies of *C. jejuni* infections in our *Sigirr*$^{-/-}$ mouse model that the primary site of *C. jejuni* infection is within the mucus layer and in the intestinal crypts, where it is in close proximity to the intestinal epithelium. The inability of the rod-shaped *C. jejuni* mutants to colonize the intestinal crypts of the *Sigirr*$^{-/-}$ mouse resulted in nonpathogenic colonization by these mutants.

The PG hydrolases Pgp1 and Pgp2 are necessary for determining the characteristic helical shape of *C. jejuni* (14, 15). The *H. pylori* PG hydrolase Csd3/HdpA is involved in creating cell curvature and twist (7), as is the *C. jejuni* homolog 1228. While the Δ*pgp1* and Δ*pgp2* mutants were rod shaped (7, 8), the Δ*1228* mutant still had a curved morphology but with decreased helical pitch that resulted in cells with a C- or S-shaped morphology. In semisolid motility agar, each of the three mutants exhibited a slight reduction in motility compared to the wild type: 81.0% for the Δ*pgp1* strain, 66.3% for the Δ*pgp2* strain, and 85.1% for the Δ*1228* strain. The observed motility defect in semisolid agar could result from either (i) the alteration in cell shape or (ii) decreased flagellar propulsion. All three mutants had wild-type flagella, as observed by electron microscopy (14, 15; also Frirdich and Gaynor, unpublished) (Fig. 1B). Moreover, if the mutants were impaired in flagellar rotation, then their motility within liquid medium, without the added viscosity of the agar, would have also been affected. In MH broth, there was little observable difference in motility between the wild type and Δ*pgp1*, Δ*pgp2*, and Δ*1228* mutant and complemented strains. This indicates that the observed reduction in motility in semisolid agar is likely due to the alterations in cell shape and not a defect in flagellar rotation, thereby affecting the strains' motility within viscous solutions.

In vitro, neither the Δ*pgp1* nor the Δ*pgp2* mutant was significantly impaired for cell adhesion, invasion, or intracellular survival (14, 15), while the Δ*1228* mutant was slightly defective at all time points (Fig. 1; also see Fig. S1 in the supplemental material). The Δ*pgp1* mutant showed an increase in IL-8 secretion in comparison to the wild type during epithelial cell infections *in vitro*, which would *in vivo* likely indicate the potential for increased inflammation (14) (see Fig. S1). In contrast, the levels of IL-8 secretion in response to the Δ*1228* mutant were decreased in comparison to the wild type. Neither the intracellular survival nor IL-8 secretion defects of the Δ*1228* mutant were restored in the Δ*1228*c complemented strain. Incubation of Δ*1228*c in the MEM used in cell culture assays resulted in a lack of complementation of the Δ*1228* strain cell shape defect, while growth of the Δ*1228*c strain in the nutrient-rich MH medium showed the restoration of wild-type morphology. This was not due to a decrease in *1228* transcriptional levels in the Δ*1228c* strain incubated in MEM and may indicate that 1228 protein function could be affected in a nutrient-limited medium.

Whereas Δ*pgp1* and Δ*pgp2* mutants displayed no loss of pathogenicity in the *in vitro* cell invasion assay, they were essentially nonpathogenic *in vivo* despite reaching a high bacterial burden. Specifically, they caused no significant pathology and were not able to colonize the intestinal crypts of infected *Sigirr*$^{-/-}$ mice. In contrast, the Δ*1228* mutant displayed little difference from the wild type *in vivo*, despite its impaired *in vitro* phenotypes. These results highlight that *in vitro* and *in vivo* data can yield different pathogenesis-related outcomes, depending on the models used for analysis. In the case of the three shape mutants described here, the ability to colonize intestinal crypts gave different results regarding pathogenicity than cell adhesion and invasion potential.

Although *in vivo* pathogen colonization and infection are a complex process, the impaired motility of the rod-shaped mutants (as assessed in semisolid agar) is likely the primary factor preventing these mutants from penetrating the mucus overlying the murine epithelium and crypts, which is required to reach the epithelium and trigger inflammation. Indeed, this layer is being increasingly appreciated for its functionality as a physical barrier to pathogen infection in the gut (38, 39). The large, interconnected mucin glycoproteins that make up the mucus layer create a thick, viscous medium that *C. jejuni* must move through. Although the Δ*pgp1* and Δ*pgp2* mutants display wild-type motility in liquid media, without the typical helical shape of *C. jejuni* and the associated corkscrew motility providing added torque to assist in their movement, they appear to be less efficient at moving through the mucus of the crypts. An added barrier to infection is the constant release of new mucins by the goblet cells into the crypts which, upon hydration, creates a flow of mucus up and out of the crypt toward the lumen. To effectively colonize the crypt, *C. jejuni* would have to maintain a velocity higher than the mucin outward flow rate to remain in the crypt. Any microbe, including those that are motile, would be pushed out of the crypt over time if its forward velocity was too low. We observed wild-type *C. jejuni* within the intestinal crypts as early as 1 day postinfection, and its presence within the intestinal crypts was maintained throughout the infection. The rod-shaped Δ*pgp1* and Δ*pgp2* mutants were relegated to the periphery of the mucus overlying the surface epithelial cells and were thus unable to interact with the epithelium of the crypts to trigger an inflammatory response. This was a characteristic in both early (1 to 3 days postinfection) and later (7 days

postinfection) stages of infection. Despite the fact that the Δ*pgp1* and Δ*pgp2* mutants showed no defect in *in vitro* adhesion, invasion, and intracellular survival in epithelial cells and some changes in host cell interactions (i.e., differential activation of Nod1 and increased IL-8 release in response to the Δ*pgp1* mutant) (14, 15), these factors do not affect the outcome of infection if the mutants are unable to reach the epithelial cells. While it is possible that the Δ*pgp1* and Δ*pgp2* mutants could be more susceptible to the action of host-produced antimicrobial peptides that would eliminate these mutants if they reached the intestinal crypts, this is unlikely as neither mutant showed increased sensitivity to any antimicrobial compounds tested *in vitro* in previous studies (14, 15).

In contrast to the rod-shaped Δ*pgp1* and Δ*pgp2* mutants, the curved Δ*1228* mutant was not impaired in its ability to colonize the mouse intestinal crypts and subsequently triggered intestinal pathology and inflammation comparable to those of the wild type. This was in spite of *in vitro* defects in epithelial cell adhesion, invasion, and intracellular survival and a decreased ability to trigger IL-8 secretion. One possible reason for why this mutant could colonize crypts whereas the rod-shaped mutants could not is that the Δ*1228* strain still maintains a curved shape and is thus still able to generate enough corkscrew motility to penetrate the mucus layer to reach the epithelial layer of the crypts. This study provides the first direct evidence that *C. jejuni*'s corkscrew motility through viscous solutions, such as mucus, mediated by its helical shape is important for ensuring that *C. jejuni* can reach and colonize intestinal crypts.

Our results further support the importance of cell shape in *C. jejuni* virulence. Although classical virulence factors such as toxins, secretion systems, and effector molecules are often the main subjects of pathogenesis research, sometimes the fundamental properties of the microbial cell, such as its cell shape, are equally as important. This is especially true of *C. jejuni*, as it expresses only a limited number of classical virulence factors. *C. jejuni* is known to be well adapted to its niche within the mammalian lower intestine and specifically in the intestinal mucus layer at the interface between the epithelium and the lumen of the intestine, where it can avoid competition with many of the resident commensal microbes. This environment contains low levels of oxygen, ideal for the microaerophilic growth requirements of *C. jejuni* (40). Moreover, being surrounded by thick and viscous mucus makes its helical shape a necessity for its motility within this layer. It appears that the ability of *C. jejuni* to colonize this niche is a key step in the ability of this pathogen to trigger gastroenteritis, likely placing *C. jejuni* into close contact with the epithelium where it activates innate immune receptors that drive the inflammatory response to infection.

The mucus layer is a major line of defense against invading enteric pathogens like *C. jejuni*. This study indicates that helical morphology is a specific bacterial adaptation required for certain bacteria, such as *C. jejuni*, to overcome this barrier and establish a successful infection. Inhibitors targeting cell shape-determining enzymes, such as the phosphinic acid-based pseudopeptide inhibitor active against *C. jejuni* Pgp1 and its homolog Csd4 in *H. pylori*, which results in cell straightening in these organisms (41), may prove to be a novel and effective therapeutic to treat infections by these helix-shaped pathogens.

ACKNOWLEDGMENTS

We thank Caixia Ma and Tina Huang for their technical assistance.

This study was supported by operating grants to E.C.G. (MOP-68981) and to B.A.V. from the Canadian Institute of Health Research (CIHR), Crohn's and Colitis Canada (CCC), and NSERC. M.S. was funded by a Michael Smith Foundation for Health Research (MSFHR) postdoctoral fellowship. B.A.V. is the Children with Intestinal and Liver Disorders (CH.i.L.D.) Foundation Research Chair in Pediatric Gastroenterology.

FUNDING INFORMATION

This work, including the efforts of Bruce A. Vallance, was funded by Gouvernement du Canada | Canadian Institutes of Health Research (CIHR) (MOP-126051). This work, including the efforts of Erin C. Gaynor, was funded by Gouvernement du Canada | Canadian Institutes of Health Research (CIHR) (MOP-68981).

REFERENCES

1. **Lawson AJ, On SL, Logan JM, Stanley J.** 2001. Campylobacter hominis sp. nov., from the human gastrointestinal tract. Int J Syst Evol Microbiol **51:**651–660. http://dx.doi.org/10.1099/00207713-51-2-651.
2. **Man SM.** 2011. The clinical importance of emerging Campylobacter species. Nat Rev Gastroenterol Hepatol **8:**669–685. http://dx.doi.org/10.1038/nrgastro.2011.191.
3. **Revez J, Schott T, Rossi M, Hanninen ML.** 2012. Complete genome sequence of a variant of Campylobacter jejuni NCTC 11168. J Bacteriol **194:**6298–6299. http://dx.doi.org/10.1128/JB.01385-12.
4. **Yang DC, Blair KM, Salama NR.** 2016. Staying in shape: the impact of cell shape on bacterial survival in diverse environments. Microbiol Mol Biol Rev **80:**187–203. http://dx.doi.org/10.1128/MMBR.00031-15.
5. **Young KD.** 2006. The selective value of bacterial shape. Microbiol Mol Biol Rev **70:**660–703. http://dx.doi.org/10.1128/MMBR.00001-06.
6. **Typas A, Banzhaf M, Gross CA, Vollmer W.** 2012. From the regulation of peptidoglycan synthesis to bacterial growth and morphology. Nat Rev Microbiol **10:**123–136. http://dx.doi.org/10.1038/nrmicro2677.
7. **Sycuro LK, Pincus Z, Gutierrez KD, Biboy J, Stern CA, Vollmer W, Salama NR.** 2010. Peptidoglycan crosslinking relaxation promotes Helicobacter pylori's helical shape and stomach colonization. Cell **141:**822–833. http://dx.doi.org/10.1016/j.cell.2010.03.046.
8. **Sycuro LK, Wyckoff TJ, Biboy J, Born P, Pincus Z, Vollmer W, Salama NR.** 2012. Multiple peptidoglycan modification networks modulate Helicobacter pylori's cell shape, motility, and colonization potential. PLoS Pathog **8:**e1002603. http://dx.doi.org/10.1371/journal.ppat.1002603.
9. **Bonis M, Ecobichon C, Guadagnini S, Prevost MC, Boneca IG.** 2010. A M23B family metallopeptidase of Helicobacter pylori required for cell shape, pole formation and virulence. Mol Microbiol **78:**809–819. http://dx.doi.org/10.1111/j.1365-2958.2010.07383.x.
10. **Kim HS, Kim J, Im HN, An DR, Lee M, Hesek D, Mobashery S, Kim JY, Cho K, Yoon HJ, Han BW, Lee BI, Suh SW.** 2014. Structural basis for the recognition of muramyltripeptide by Helicobacter pylori Csd4, a D,L-carboxypeptidase controlling the helical cell shape. Acta Crystallogr D Biol Crystallogr **70:**2800–2812. http://dx.doi.org/10.1107/S1399004714018732.
11. **Sycuro LK, Rule CS, Petersen TW, Wyckoff TJ, Sessler T, Nagarkar DB, Khalid F, Pincus Z, Biboy J, Vollmer W, Salama NR.** 2013. Flow cytometry-based enrichment for cell shape mutants identifies multiple genes that influence Helicobacter pylori morphology. Mol Microbiol **90:**869–883. http://dx.doi.org/10.1111/mmi.12405.
12. **Kim HS, Im HN, An DR, Yoon JY, Jang JY, Mobashery S, Hesek D, Lee M, Yoo J, Cui M, Choi S, Kim C, Lee NK, Kim SJ, Kim JY, Bang G, Han BW, Lee BI, Yoon HJ, Suh SW.** 2015. The cell shape-determining Csd6 protein from Helicobacter pylori constitutes a new family of L,D-carboxypeptidase. J Biol Chem **290:**25103–25117. http://dx.doi.org/10.1074/jbc.M115.658781.
13. **An DR, Kim HS, Kim J, Im HN, Yoon HJ, Yoon JY, Jang JY, Hesek D, Lee M, Mobashery S, Kim SJ, Lee BI, Suh SW.** 2015. Structure of Csd3 from Helicobacter pylori, a cell shape-determining metallopeptidase. Acta Crystallogr D Biol Crystallogr **71:**675–686. http://dx.doi.org/10.1107/S1399004715000152.
14. **Frirdich E, Biboy J, Adams C, Lee J, Ellermeier J, Gielda LD, Dirita VJ, Girardin SE, Vollmer W, Gaynor EC.** 2012. Peptidoglycan-modifying

enzyme Pgp1 is required for helical cell shape and pathogenicity traits in Campylobacter jejuni. PLoS Pathog **8:**e1002602. http://dx.doi.org/10.1371/journal.ppat.1002602.

15. **Frirdich E, Vermeulen J, Biboy J, Soares F, Taveirne ME, Johnson JG, DiRita VJ, Girardin SE, Vollmer W, Gaynor EC.** 2014. Peptidoglycan LD-carboxypeptidase Pgp2 influences Campylobacter jejuni helical cell shape and pathogenic properties and provides the substrate for the DL-carboxypeptidase Pgp1. J Biol Chem **289:**8007–8018. http://dx.doi.org/10.1074/jbc.M113.491829.
16. **Lertsethtakarn P, Ottemann KM, Hendrixson DR.** 2011. Motility and chemotaxis in Campylobacter and Helicobacter. Annu Rev Microbiol **65:**389–410. http://dx.doi.org/10.1146/annurev-micro-090110-102908.
17. **Hermans D, Van Deun K, Martel A, Van Immerseel F, Messens W, Heyndrickx M, Haesebrouck F, Pasmans F.** 2011. Colonization factors of Campylobacter jejuni in the chicken gut. Vet Res **42:**82. http://dx.doi.org/10.1186/1297-9716-42-82.
18. **Stahl M, Ries J, Vermeulen J, Yang H, Sham HP, Crowley SM, Badayeva Y, Turvey SE, Gaynor EC, Li X, Vallance BA.** 2014. A novel mouse model of Campylobacter jejuni gastroenteritis reveals key pro-inflammatory and tissue protective roles for Toll-like receptor signaling during infection. PLoS Pathog **10:**e1004264. http://dx.doi.org/10.1371/journal.ppat.1004264.
19. **Wassenaar TM, van der Zeijst BA, Ayling R, Newell DG.** 1993. Colonization of chicks by motility mutants of Campylobacter jejuni demonstrates the importance of flagellin A expression. J Gen Microbiol **139:**1171–1175. http://dx.doi.org/10.1099/00221287-139-6-1171.
20. **Guerry P.** 2007. Campylobacter flagella: not just for motility. Trends Microbiol **15:**456–461. http://dx.doi.org/10.1016/j.tim.2007.09.006.
21. **Svensson SL, Pryjma M, Gaynor EC.** 2014. Flagella-mediated adhesion and extracellular DNA release contribute to biofilm formation and stress tolerance of Campylobacter jejuni. PLoS One **9:**e106063. http://dx.doi.org/10.1371/journal.pone.0106063.
22. **Konkel ME, Klena JD, Rivera-Amill V, Monteville MR, Biswas D, Raphael B, Mickelson J.** 2004. Secretion of virulence proteins from Campylobacter jejuni is dependent on a functional flagellar export apparatus. J Bacteriol **186:**3296–3303. http://dx.doi.org/10.1128/JB.186.11.3296-3303.2004.
23. **Kaiser GE, Doetsch RN.** 1975. Letter: enhanced translational motion of Leptospira in viscous environments. Nature **255:**656–657. http://dx.doi.org/10.1038/255656a0.
24. **Kan W, Wolgemuth CW.** 2007. The shape and dynamics of the Leptospiraceae. Biophys J **93:**54–61. http://dx.doi.org/10.1529/biophysj.106.103143.
25. **Magariyama Y, Kudo S.** 2002. A mathematical explanation of an increase in bacterial swimming speed with viscosity in linear-polymer solutions. Biophys J **83:**733–739. http://dx.doi.org/10.1016/S0006-3495(02)75204-1.
26. **Ferrero RL, Lee A.** 1988. Motility of Campylobacter jejuni in a viscous environment: comparison with conventional rod-shaped bacteria. J Gen Microbiol **134:**53–59.
27. **Szymanski CM, King M, Haardt M, Armstrong GD.** 1995. Campylobacter jejuni motility and invasion of Caco-2 cells. Infect Immun **63:**4295–4300.
28. **Sham HP, Yu EY, Gulen MF, Bhinder G, Stahl M, Chan JM, Brewster L, Morampudi V, Gibson DL, Hughes MR, McNagny KM, Li X, Vallance BA.** 2013. SIGIRR, a negative regulator of TLR/IL-1R signalling promotes microbiota dependent resistance to colonization by enteric bacterial pathogens. PLoS Pathog **9:**e1003539. http://dx.doi.org/10.1371/journal.ppat.1003539.
29. **van Putten JP, van Alphen LB, Wosten MM, de Zoete MR.** 2009. Molecular mechanisms of *Campylobacter* infection. Curr Top Microbiol Immunol **337:**197–229. http://dx.doi.org/10.1007/978-3-642-01846-6_7.
30. **Young KT, Davis LM, Dirita VJ.** 2007. Campylobacter jejuni: molecular biology and pathogenesis. Nat Rev Microbiol **5:**665–679. http://dx.doi.org/10.1038/nrmicro1718.
31. **Khan MA, Steiner TS, Sham HP, Bergstrom KS, Huang JT, Assi K, Salh B, Tai IT, Li X, Vallance BA.** 2010. The single IgG IL-1-related receptor controls TLR responses in differentiated human intestinal epithelial cells. J Immunol **184:**2305–2313. http://dx.doi.org/10.4049/jimmunol.0900021.
32. **Maue AC, Mohawk KL, Giles DK, Poly F, Ewing CP, Jiao Y, Lee G, Ma Z, Monteiro MA, Hill CL, Ferderber JS, Porter CK, Trent MS, Guerry P.** 2013. The polysaccharide capsule of Campylobacter jejuni modulates the host immune response. Infect Immun **81:**665–672. http://dx.doi.org/10.1128/IAI.01008-12.
33. **Stahl M, Vallance BA.** 2015. Insights into Campylobacter jejuni colonization of the mammalian intestinal tract using a novel mouse model of infection. Gut Microbes **6:**143–148. http://dx.doi.org/10.1080/19490976.2015.1016691.
34. **Van Deun K, Pasmans F, Ducatelle R, Flahou B, Vissenberg K, Martel A, Van den Broeck W, Van Immerseel F, Haesebrouck F.** 2008. Colonization strategy of Campylobacter jejuni results in persistent infection of the chicken gut. Vet Microbiol **130:**285–297. http://dx.doi.org/10.1016/j.vetmic.2007.11.027.
35. **Bereswill S, Fischer A, Plickert R, Haag LM, Otto B, Kuhl AA, Dasti JI, Zautner AE, Munoz M, Loddenkemper C, Gross U, Gobel UB, Heimesaat MM.** 2011. Novel murine infection models provide deep insights into the "menage a trois" of Campylobacter jejuni, microbiota and host innate immunity. PLoS One **6:**e20953. http://dx.doi.org/10.1371/journal.pone.0020953.
36. **Hugdahl MB, Beery JT, Doyle MP.** 1988. Chemotactic behavior of Campylobacter jejuni. Infect Immun **56:**1560–1566.
37. **Stahl M, Friis LM, Nothaft H, Liu X, Li J, Szymanski CM, Stintzi A.** 2011. L-fucose utilization provides Campylobacter jejuni with a competitive advantage. Proc Natl Acad Sci U S A **108:**7194–7199. http://dx.doi.org/10.1073/pnas.1014125108.
38. **Bergstrom KS, Kissoon-Singh V, Gibson DL, Ma C, Montero M, Sham HP, Ryz N, Huang T, Velcich A, Finlay BB, Chadee K, Vallance BA.** 2010. Muc2 protects against lethal infectious colitis by disassociating pathogenic and commensal bacteria from the colonic mucosa. PLoS Pathog **6:**e1000902. http://dx.doi.org/10.1371/journal.ppat.1000902.
39. **Zarepour M, Bhullar K, Montero M, Ma C, Huang T, Velcich A, Xia L, Vallance BA.** 2013. The mucin Muc2 limits pathogen burdens and epithelial barrier dysfunction during Salmonella enterica serovar Typhimurium colitis. Infect Immun **81:**3672–3683. http://dx.doi.org/10.1128/IAI.00854-13.
40. **Woodall CA, Jones MA, Barrow PA, Hinds J, Marsden GL, Kelly DJ, Dorrell N, Wren BW, Maskell DJ.** 2005. Campylobacter jejuni gene expression in the chick cecum: evidence for adaptation to a low-oxygen environment. Infect Immun **73:**5278–5285. http://dx.doi.org/10.1128/IAI.73.8.5278-5285.2005.
41. **Liu Y, Frirdich E, Taylor JA, Chan AC, Blair KM, Vermeulen J, Ha R, Murphy ME, Salama NR, Gaynor EC, Tanner ME.** 2016. A bacterial cell shape-determining inhibitor. ACS Chem Biol **11:**981–991. http://dx.doi.org/10.1021/acschembio.5b01039.